

Light Echo Modeling of the Active Galactic Nucleus NGC 3783 Using TORMAC - WORKING DRAFT

Zachary Knutson,¹★ Triana Almeyda,¹ Andrew Robinson² Sebastian Hönig³ and Jack Gallimore⁴

¹*Department of Astronomy, University of Florida, 211 Bryant Space Science Center, Gainesville, FL, 32611, USA*

²*School of Physics and Astronomy, Rochester Institute of Technology, 1 Lomb Memorial Drive, Rochester, NY 14623, USA*

³*Department of Physics & Astronomy, University of Southampton, Southampton, SO17 1BJ, UK*

⁴*Department of Physics, Bucknell University, Lewisburg, PA 17837, USA*

Accepted XXX. Received YYY; in original form ZZZ

ABSTRACT

When supermassive black holes, found in the center of most galaxies, rapidly consume material, they are known as active galactic nuclei (AGN). This study employs computational modeling to explore the dust structure commonly found around AGN, focusing on one such AGN, NGC 3783. Utilizing the TORMAC code developed by Dr. Triana Almeyda, we generate simulated infrared (IR) light curves based on a 3D ensemble of clouds within a simulated dust structure, using observed optical light curves of NGC 3783 as the input continuum source. We use a Markov Chain Monte Carlo (MCMC) code, written by collaborator Dr. Jack Gallimore, to determine the best-fit parameters of the dust distribution by comparing the simulated IR light curves to the observed IR light curves for NGC 3783. Here we present preliminary results from these simulations and demonstrate their application towards constraining the structure and geometry of NGC 3783. [instead of what was here, add some discussion / key findings]

Key words: radiative transfer – galaxies: active

1 INTRODUCTION

At the center of most galaxies resides a super massive black hole (SMBH) with masses typically exceeding $10^6 M_\odot$. When these SMBHs rapidly accrete surrounding gas and dust, they are classified as active galactic nuclei (AGN). Close to the center of these AGN, fueled primarily by the gravitational potential energy of the infalling material, a relatively small disk (the accretion disk) of super heated plasma emits primarily in the X-ray, ultraviolet (UV), and optical portions of the electromagnetic (EM) spectrum. These AGN have luminosities typically between 10^{40} ergs•s⁻¹ and 10^{47} erg•s⁻¹ and can, in some cases, exceed the luminosity of the host galaxy. Surrounding this accretion disk is a much larger structure of dust, which, when heated by the accretion disk, emits primarily in the infrared (IR). Understanding the structure and geometry of this dust provides insights into the growth and evolution of SMBHs and how AGN interact more broadly with their host galaxies allowing for a greater understanding of the processes governing galactic evolution. [Zach: Need to revise this to be a little more specific. Definitely glossing over a lot of stuff that should be cited/quantified.]

However, due to the milliarcsecond spatial resolution required to directly resolve the inner radius of the dust distributions in even the closest AGN, any attempts to understand the hottest portion of the dust currently require some form of modeling. [Zach: Citeeee] Multiple successful attempts have been made to resolve the inner radius of several close AGN utilizing IR interferometry, but this method does not extend well to AGN of higher redshift. [Cited in Almeyda et al. 2017; Swain et al. 2003; Kishimoto et al. 2009; Pott et al. 2010;

Kishimoto et al. 2011; Weigelt et al. 2012], [Cited in Almeyda et al. 2020: e.g., Kishimoto et al. 2011; Burtscher et al. 2013] [Zach: This needs to be expanded to actually say what these people did]

Instead, an alternative approach, based on reverberation mapping, uses both optical and IR wavelengths to bypass the need for high resolution imaging by utilizing the time domain. [Zach: Instead of just jumping into saying this method exists, maybe cite a time / the times when this was first used?] The driving principle of dust reverberation mapping is that the IR continuum response is delayed relative to the optical continuum emission since the optical light from the accretion disk must first travel to the dust where it is absorbed and then re-emitted in the IR along the observer's path. [Zach: Theory of reverberation mapping says that Theory of reverberation mapping how do we implement it observationally how do we extend it to modeling]

Observational reverberation mapping is commonly used to constrain the characteristic size of the torus [refs] by determining the average[?] delay between the optical and IR light curves, then converting this time delay into a characteristic radius. In an attempt to gain additional information about the structure and geometry of the circumnuclear dust, we also consider that the total IR response at any given time is a summation of partial responses to the optical emission at all time delays. This means that the optical emission and IR response will not be perfectly correlated. We can instead model the IR response light curve as a convolution of the optical emission with a “transfer function”. This transfer function then would contain information about the structure and geometry of the dust.

In an attempt to gain more information about the structure, However, since the observed light curve is a convolution with the transfer function transfer function contains information about the structure

* E-mail: zach.knutson7431@gmail.com

and geometry of the torus we can use the transfer function to learn more about the

Start the other way: we know that from reverberation mapping - transfer function - transfer function contains information - extract that information using modeling

The forward modeling code TORMAC (TOrus Reverberation MAppling Code) has previously been employed to simulate the multi-wavelength response from a circumnuclear dust distribution to a delta function “pulse”, emulating that dust configuration’s “transfer function” (Almeyda et al. 2017, 2020). However, it is also capable of generating IR response light curves to observed input optical light curves. [Zach: I think you reminded me a while ago that TORMAC has already done this, need to rephrase] In this paper, we utilize TORMAC to extract additional information about the dust structure of a well-studied AGN, NGC 3783.

IR interferometric observations of NGC 3783 have revealed the presence of a hot, compact, disk-like structure, commonly referred to as the “dusty torus” and a cooler, resolved, extended component in the polar regions (GRAVITY Collaboration 2021 [among others]). A significant fraction of the IR emission from NGC 3783 comes from this polar dust structure, which we refer to as the “polar bi-cone”. Both IR interferometry and SED model fitting [reffssss] have been used to gain information about NGC 3783’s circumnuclear dust, but this paper serves as the first use of light curves to extract additional information about the circumnuclear dust.

2 METHODS

NGC 3783 has been observed in the B band (optical) as well as the J, H, and K bands (IR response) from 2006 to 2011 with an average cadence of 4.5 days during the observing season (Lira et al. 2011). These resulting light curves have been host galaxy corrected. Since these light curves contain large gaps between observing seasons, the B band light curve is interpolated using the power spectrum derived from the data. The interpolated B band light curve is used as an input to TORMAC (see Section 2.1), representing the variations of the central source. The J, H, and K band light curves are compared to the model light curves TORMAC produces. Therefore, it is used as an input to our MCMC parameter estimation code tormacFit. (see Section 2.2).

2.1 IR Light Curve Model Creation: TORMAC

Since TORMAC has already been introduced in Almeyda et al. (2017), and expanded in Almeyda et al. (2020), here we will provide an overview of TORMAC’s primary functions and new capabilities. TORMAC simulates the IR response from the circumnuclear dust surrounding AGN as a 3D ensemble of dust clouds, randomly distributed within user defined geometries. TORMAC models the torus as a clumpy, flared disk with linear scale height. Because classical clumpy torus models are unable to model extended polar mid-IR emission from AGNs, TORMAC is now also capable of simulating clumpy polar dust structures. The number of clouds contained within both structures can be defined by the user, with a canonical value of $N_{cl} = 10^5$ being used in all models presented in this paper. The fraction of the clouds which reside in the torus is given by the user defined parameter f_{cl} , where $f_{cl} = 0$ corresponds to all of the clouds residing in the polar dust structure. Both structures are oriented to the observer by the user defined inclination angle i , such that when $i = 90^\circ$, the torus structure is edge on, and when $i = 0^\circ$, the observer’s line of sight passes through the center of the polar dust structure. A

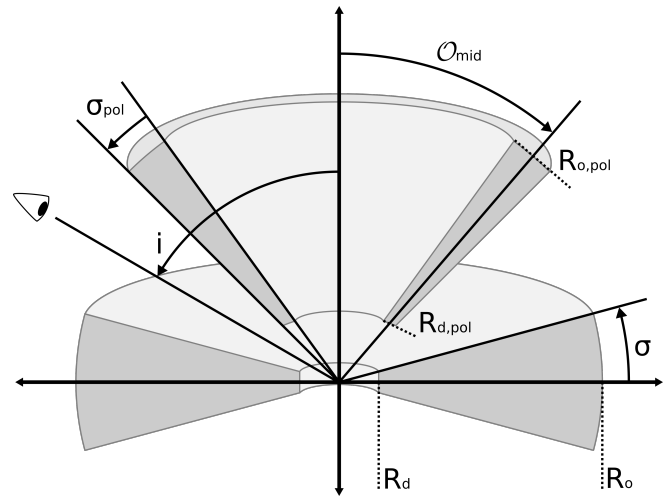


Figure 1.

cloud’s position (in either structure) is defined by its distance from the central illuminating source r , its polar angle θ (where $\theta = 0^\circ$ and $\theta = 180^\circ$ are defined as the polar axes), and its azimuthal angle ϕ .

The torus’ geometry extends from the dust sublimation radius R_d to an outer radius R_o . R_o is determined by the user defined parameter Y , where $Y = R_o/R_d$. Radially from the central source, clouds in the torus are arranged following a power-law distribution with user defined index p , where $N_{cl}(r) \propto r^{p-2}$. The half angular width of the torus is determined by the user defined parameter σ . In polar angle, clouds follow a Gaussian distribution centered in the equatorial plane ($\theta = 90^\circ$) and with standard deviation σ , such that the polar angle distribution is defined as:

$$N_{cl}(\theta) \propto \exp[-(\theta - 90^\circ)^2/2\sigma^2]$$

The user also must define the fraction of the torus volume which is filled with clouds, $\log(\Phi)$. If $\log(\Phi) = 0.01$, 1% of the torus’ volume will contain clouds.

The polar dust structure is modeled as a hollow bi-cone with the user defined opening angle O_{mid} . The polar dust is similarly generated based on the analogous user defined parameters Y_{pol} , p_{pol} , σ_{pol} , and $\log(\Phi_{pol})$. Radially, the polar dust extends from R_d to $R_{o,pol}$, with $Y_{pol} = R_{o,pol}/R_d$. Clouds in the polar dust are also arranged following a power-law distribution with $N_{cl}(r) \propto r^{p_{pol}-2}$. However, in polar angle, the distribution of polar dust clouds is the sum of two Gaussian distributions, centered at $\theta = 0 + O_{mid}$ and $\theta = 180 - O_{mid}$. Both Gaussian distributions have standard deviation σ_{pol} . This yields the polar angle distribution:

$$N_{cl}(\theta) \propto \exp[-(\theta - O_{mid})^2/2\sigma_{pol}^2] + \exp[-(\theta - (180 - O_{mid}))^2/2\sigma_{pol}^2]$$

The dust clouds are heated either directly by the UV/optical continuum emitted from the accretion disk or, if shadowed [Zach: what is shadowing?], indirectly by the diffuse radiation field produced by the directly illuminated clouds. The illuminating AGN radiation field may be anisotropic, due to “edge darkening” of the accretion disk. Therefore, the AGN luminosity is assumed to have the following polar angle dependence:

$$L(\theta) = [s + (1 - s)(1/3)(1 + 2 \cos \theta) \cos \theta] L_{AGN}$$

(see Netzer 1987), where L_{AGN} is the isotropic bolometric luminosity of the AGN and the “softening parameter” s determines the degree of anisotropy with an s value of 1.0 corresponding to isotropic

illumination. In the isotropic case, R_d is a constant value, only dependent on the dust's sublimation temperature T_{sub} . However, in the anisotropic case $s < 1$, R_d is instead a function of both the dust sublimation temperature, T_{sub} , and θ . For the purposes of calculating R_o , the isotropic R_d is always used in the expression of Y .

[Insert brief overview of new grain stuff] [Zach: This needs to contain a reference to sebs paper so we can talk about the cloud grids.] [Zach: Also needs to have the dust sublimation radius equation]

TORMAC also calculates the anisotropic emission from individual clouds, as the illuminated face of a cloud will have a higher temperature than the non-illuminated side, see Section 2.4 of Almeyda et al. (2017). Additionally, the emission from any given cloud is also subject to two “global” opacity effects. The first is cloud shadowing, whereby an outer cloud has its line of sight to the central AGN continuum source blocked by one or more inner clouds, closer to the central source. Clouds that are shadowed in this way are heated indirectly by the diffuse radiation emitted by surrounding directly illuminated clouds (see Almeyda et al. (2017)). Between Almeyda et al. (2020) and this paper, the implementation of cloud shadowing in TORMAC has changed, and is described in detail in Section 2.1.1. The second is cloud occultation, whereby the emitted spectrum of a cloud may be attenuated by clouds intervening along the line of sight to the observer (see Section 2.1 in Almeyda et al. (2020)). [Zach: I definitely think this paragraph should move before the description of illumination, thoughts?]

2.1.1 Modified Cloud Shadowing

In Almeyda et al. (2017, 2020), an analytic approximation is used to calculate the probability that a cloud at a given radius will be shadowed. While this approximation may be sufficient for many cases, it often overestimates the number of clouds shadowed, with some extreme cases exacerbating this effect. In the past, TORMAC has used this probabilistic approach to reduce model execution time, but due to general improvements in TORMAC’s model execution time, it has become computationally feasible to accurately determine which clouds are shadowed.

We compute each cloud’s shadow as a cone that extends from its surface to infinity with a constant solid angle as observed from the central source. To determine if a given cloud is shadowed, we determine which of these cones the cloud intersects, and the area of intersection is calculated and summed. A cloud is considered shadowed if its intersection area is greater than 50% of its total area. If a cloud is considered shadowed, it will only be illuminated by diffuse radiation, whereas if it is not shadowed, it will only be directly illuminated by the central source. [Zach: Make clear that intersection area must be greater than 50% for an individual cone not the sum] For shadowed clouds, the total intersection area is then used to compute the cloud’s attenuated radius from the central source according to the equation

$$R_{\text{att}} = R_{\text{cl}} \cdot \exp(A_{\text{int}}/2A_{\text{cl}})$$

where R_{cl} is the physical radius from the central source of the cloud, A_{int} is the total intersection area, and A_{cl} is the area of the cloud. The attenuated radius is then used to determine the amount of diffuse radiation expected, based off of a precomputed cloud grid. [Zach: What is this precomputed grid? Say that it is based off of the clouds distance and wavelength] [Zach: need to better explain what the “attenuated radius” means]

2.2 MCMC Model Fitting Using tormacFit

[Zach: Would probably be better to say something along the lines of: To rapidly sample the goodness of fit of our models across the parameter space to the ground truth observed data, we use mcmc...] As a way to estimate the constraints on the parameters for which we generate TORMAC models, we employ Markov Chain Monte Carlo (MCMC) modeling to fit the IR response models generated by TORMAC to the observations. We use a code entitled tormacFit, which is a heavily modified version of clumpyDREAM (Sales et al. 2015), to perform the MCMC search. [Zach: Probably should just cite pydream] The fitter calculates the likelihood using a χ^2 test using all of the points in the observed light curve. [Zach: Can revise this to better show mathematically what our log liklihood looks like] Since TORMAC is capable of calculating light curves for multiple wavelengths, and multiple observed wavebands (J, H, and K) are available for NGC 3783, tormacFit was made to handle multi-wavelength fitting. The likelihoods calculated for each wavelength are multiplied to arrive at the final likelihood used for the MCMC search. [Zach: Can just say that the code jointly fits the wavelengths] For all of the posterior distributions presented in Section 3, we fit to both the H and K bands. We were unable to properly fit the light curves to the J band, explained in Section 4. [Zach: This is a poor location to put this info...]

We introduce two additional parameters to our MCMC search: log(amp) and Sys. Unc. (%). The log(amp) parameter is a monochromatic scaling factor applied to the model lightcurve, used to . log(amp) values far from unity represent limitations of TORMAC to reproduce the true observed flux, or additional sources of extinction which have not been considered. The Sys. Unc. (%) parameter is systematic uncertainty added to the uncertainty on the fluxes for the observed light curve, and represents additional random, yet unexplained fluctuations introduced during reprocessing of the optical radiation. [Zach: this is not a good way to explain systematic uncertainty]

To perform the MCMC search, we calculate a set of TORMAC models which sample the parameter space on a regular grid. For MCMC proposal evaluations which do not lie on one of these grid points, the model light curve is nd-linearly interpolated between adjacent grid points. Therefore, we impose that all of our model grids are “regular”, meaning that the set of models we run is the cartesian product of all of the sets containing a respective parameter’s values to be tested, i.e., there are no gaps in the grid.

3 RESULTS OF MCMC PARAMETER ESTIMATION

As discussed in Section 2.1, TORMAC is able to model the IR response from an AGN, producing the response IR light curve from the input optical light curve. In Section 4, we present some of the simulated responses to optical light curves from Lira et al. (2011) of NGC 3783. Instead, in this section, we focus on the resulting parameter estimations from a variety of modeled dust cloud distributions to the observed light curves. The dust distributions and number of free parameters grow in complexity throughout the section in order to individually investigate the influence in adding the more complex dust distributions to the parameter estimations/fits. [Zach: Dont know what to say instead but feel like can justify better why increasing complexity] For instance, in Section 3.1 we explore the model fits of a torus only dust distribution. In Section 3.2, we explore the inclusion of a polar distribution while reducing the overall complexity of the grids first by generating a grid that ties the TORMAC parameters of both components, then by generating a grid that varies the

Table 1. Parameter values used to construct the torus only model grid. Parameter values represent points on a regular grid with no gaps, ie. all possible combinations of parameters are evaluated. ¹ only grid(s) which allow for uncapped polar cloud sizes. ² note that the polar parameters are proportional to the torus, ie. $Y10$ and $Y_{\text{pol}}20$ was run, $Y10$ $Y_{\text{pol}}50$ was not run. ³ right now only for $f_{\text{cl}}0.333$.

Parameter	Torus Only	Torus & Prop. Polar ²	Torus Conf. 1	Torus Conf. 2	Fig 6	Fig 7	Fig 8,9,10 ¹
Y	10, 25, 50, 75, 100, 500	10, 25, 50, 75, 100	10	25	5, 50, 100	5, 10, 25, 50, 100	2, 5, 10, 25, 50
σ	5, 10, 30, 45	5, 10, 30, 45	5	5	5, 25, 45	5, 10, 15, 25	2, 5, 10, 20
p	-2, -1, 0, 1, 2	-2, -1, 0, 1, 2	1	0	-2, 0, 2	-2, 0, 2	-1, 0, 1, 2
$\log(\Phi)$	-1, -2, -3, -4	-1, -2, -3, -4	-2	-4	-1, -2, -3, -4	-1, -2, -3, -4	-1, -2, -3, -4
i	0, 30, 45, 60, 90	0, 30, 45, 60, 90	20, 50, 100, 150, 200	0, 30, 45, 60, 90	0, 30, 45, 60, 75	0, 30, 45, 60, 75	0, 30, 45, 60, 75
s	1.0 (iso), 0.1 (aniso)	1.0, 0.1	0.1	0.1	1.0, 0.1	0.1	1.0 ³ , 0.1
Y_{pol}	–	20, 50, 100, 150, 200	20, 50, 100, 150, 200	5, 100, 200	5, 50, 100, 200	5, 50, 100	5, 50, 100
σ_{pol}	–	2, 4, 12, 18	2, 4, 12, 18	2, 5, 10, 15	2, 10, 20		
P_{pol}	–	-2, -1, 0, 1, 2	-2, -1, 0, 1, 2	-2, 0, 2	-1, 0, 1, 2		
$\log(\Phi_{\text{pol}})$	–	-1, -2, -3, -4	-1, -2, -3, -4	-1, -2, -3, -4	-1, -2, -3, -4	-1, -2, -3, -4	-1, -2, -3, -4
O_{mid}	–	10, 30	10, 30	10, 22.5, 35	22.5, 35, 45	10, 25, 40	
f_{cl}	–	?	0.333, 0.5, 0.667, 0.9	0.333	0.333?, 0.667?	0.333, 0.667	
numclouds	50000	50000	50000	50000	100000	100000	100000

polar components while keeping the torus components fixed. Lastly, Section 3.3 contains model grids that vary all of the available parameters in both cloud distributions to properly sample the entire possible parameter space.

3.1 Torus Only Models

AGN circumnuclear dust has typically been modeled as a single compact disk component. We investigate if a single torus component will yield model IR light curves that sufficiently match the observed IR light curves. [Zach: also have a hunch can say this better] The geometric parameters of the torus (Y , σ , i , and s) as well as the structural parameters (p and $\log(\Phi)$) were varied independently, such that all possible combinations of the parameter values are sampled, herein referred to as a "regular grid". The grid is finely sampled over these parameters, with a complete set of parameter values enumerated in Table 1. No priors were applied in the analysis of this grid, and the ranges of these parameters represent generous limits as to sample all reasonably possible torus combinations. [Zach: Uniform priors not no priors also move to sec 2.2 also bad phrasing on the last part of this sentence]

From this grid, tormacFit was used to compute two separate sets of posterior distributions, corresponding to the isotropic models ($s=1.0$) and the anisotropic models ($s=0.1$). This was done to distinguish the influence from the type of illumination of the dust distribution from the rest of the parameters. The posterior distributions generated from the isotropic models are shown in Figure 2.

In the top right panel of Figure 1, the volume filling factor ($\log(\Phi)$), shown in log, is tightly constrained, with most samples ranging between 0.6% and 0.3% of the torus' volume containing clouds. In the left panel of the second row, the radial cloud distribution (p) is also tightly constrained around $p=1$. In the center panel, the inclination of the torus is also constrained to between approximately 57° and 67° (moderately inclined). In contrast, the right panel of the second row corresponding to the radial extent of the disk (Y),

is unconstrained as most samples tend to favor models at the lower bound of the parameter space ($Y \approx 10R_d$) explored. Similarly, in the bottom left panel, the angular width of the torus (σ) is also unconstrained, with most samples also favoring the lower bound of the parameter space ($\sigma \approx 5^\circ$). [Zach: want to do something like above with all other grid. Give specific and general info. want to format it sorta like X is Y+Z, which is very constrained.]

Both parameter estimations generally favor a compact (low Y), thin (low σ), torus with clouds taking up of order 0.1% to 1% of the torus volume (moderate $\log(\Phi)$). They also favor a moderately inclined torus with the clouds somewhat centrally distributed in volume ($p \approx 1$). The results from a torus only dust distribution showed that some of our parameters did not converge and favored the lower edge of the explored parameter space (notably Y and σ). Therefore, the models with a torus only component are not sufficient to explain the observed light curves and we widened our parameter space by including a polar dust distribution in addition to the torus. [Zach: this is not WHY the models cannot explain the observed light curves, it is that there is a large amount of systematic error in our lightcurve still! Would be good to quantify the goodness of fit (we can do this)]

3.2 Introduction of Polar Dust

In our second model set, we explore a dust distribution with both torus and polar dust components. One of the largest challenges with sampling the torus and polar dust parameter space is that many more degrees of freedom are introduced. We choose to reduce the number of free parameters by equating the relevant polar parameters to the equivalent torus parameters. For instance, in Table ??, p/p_{pol} , Y/Y_{pol} , $\sigma/\sigma_{\text{pol}}$, and $\log(\Phi)/\log(\Phi_{\text{pol}})$ have been paired, reducing the number of free parameters from 11 to 7. While we do not necessarily expect these parameters to be this correlated in AGN, this model grid is an initial attempt to introduce polar dust into our parameter estimation without adding too many degrees of freedom at once.

In addition to the parameters which define the polar dust distribu-

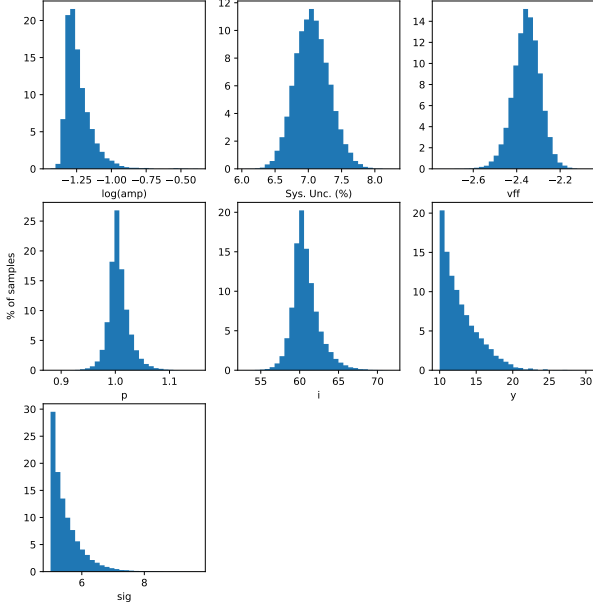


Figure 2. Posterior distribution generated by iterating tormacFit on the isotropic models from the initial torus only grid of models. Bar height corresponds to posterior probability. $\log(\text{amp})$ and Sys. Unc. (%) represent the free parameters introduced in Section 2.2, while the remaining panels enumerate all of the free parameters of the grid (see Table 1). [Zach: Why only showing isotropic?]

tion, an additional parameter, opening angle (O_{mid}) is also introduced (see Section 2.1).

Similar to the previous torus only models, tormacFit was run for both the isotropic models and the anisotropic models, producing two different posterior distributions. In Figure 3, we only show the posterior distribution results from the isotropic models. [Zach: Why?]

Compared to the posterior distributions shown in Figure 2, adding the proportional polar dust distribution resulted in a larger but more centrally located cloud distribution (lower p & p_{pol} , higher Y & Y_{pol}), a lower density (low $\log(\Phi)$ & $\log(\Phi_{\text{pol}})$), and higher inclinations (edge on) being favored. These models also support larger opening angles. [Zach: Should I expand the best fit ranges for all of the grids or make them all like this?]

Despite the introduction of a polar dust distribution, σ , and now i , $\log(\Phi)$, and O_{mid} are now unconstrained, with most models favoring edge of the explored parameter ranges. [Zach: particularly dont like saying "most models favor the edge" can say this differently] We therefore determine that a torus and wind distribution with each of their respective parameters tied in value to each other is not sufficient to determine a unique, physically realistic fit to the data. Next, we explore varying more parameters of the polar dust structure.

In the next set of models, we vary the polar dust structure parameters while holding the torus structure fixed. Table ?? shows the parameters of the grids of models were generated for each of the two fixed tori examined. The two torus configurations were determined from the peak of the posterior distributions of the previous model grids. The wind parameter values match the parameter values examined in the previous set of models. In addition, we add another free parameter, the cloud fraction, defined as f_{cl} , corresponding to the fraction of clouds present in the torus versus the wind distributions. In the previous model grids, we adopted a standard of 67%

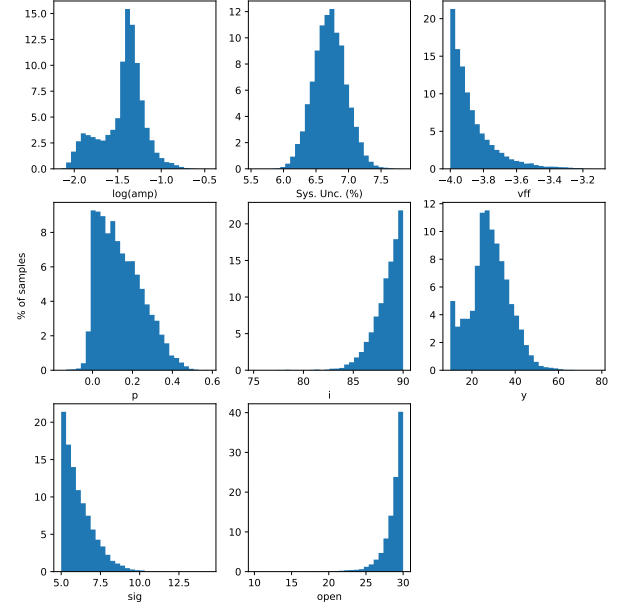


Figure 3. Like Figure 2, this posterior distribution represents the results generated by tormacFit using the torus and proportional wind model grid. Note the additional parameter " O_{mid} ". Because the wind parameters are proportional to the torus parameters, only the torus parameters are shown, but the wind parameters can be derived by comparing the posteriors with Table ??.

of the clouds in the torus, and 33% of the clouds distributed equally between the top and bottom sections of the polar bi-cone. A cloud fraction of 1 represents all of the clouds residing in the torus, while a cloud fraction of 0 represents placing all of the clouds in the polar bi-cone. [Zach: isnt this already in the code review?]

Both posterior distributions, Figure 4 ("Torus 1") and Figure 5 ("Torus 2"), were generated using tormacFit by the same method as the previous model grids. We find that the wind distributions for both torus configurations vary significantly from the "proportional" parameter values tested before. In particular, Torus 1 shows significant bimodality in its inclination posterior distribution, favoring both lower, moderate inclinations ($i \approx 30^\circ$) as well as higher inclinations ($i \approx 60^\circ$). This bimodal degeneracy can be seen across multiple parameters. For both torus configurations, but especially Torus 1, more of the posterior samples fall within the parameter space. Still, O_{mid} (Torus 1 & 2) as well as $\log(\Phi_{\text{pol}})$, Y_{pol} , and f_{cl} (Torus 2) favor the edge of the parameter space. Despite using a torus based on the peak of the previous model grid's posteriors, the modification of Torus 2's wind modified the most favored inclination from completely edge on to a more moderate inclination.

Generally, the most samples across both posterior distributions favor an extended wind (roughly 10 times larger than the torus for Torus 1, and roughly twice as large as the torus for Torus 2) and a moderately centrally located polar cloud distribution ($p_{\text{pol}} \approx 0$). Torus 1's wind is better constrained, demonstrated by the narrower peaks in multiple parameters across the posterior distributions. Both winds favor a large fraction of the clouds residing in the wind.

3.3 Variable Torus and Polar Dust Models

In Sections 3.1 and 3.2, we have shown that trying to limit the number of free parameters does not enable us to conclusively constrain the

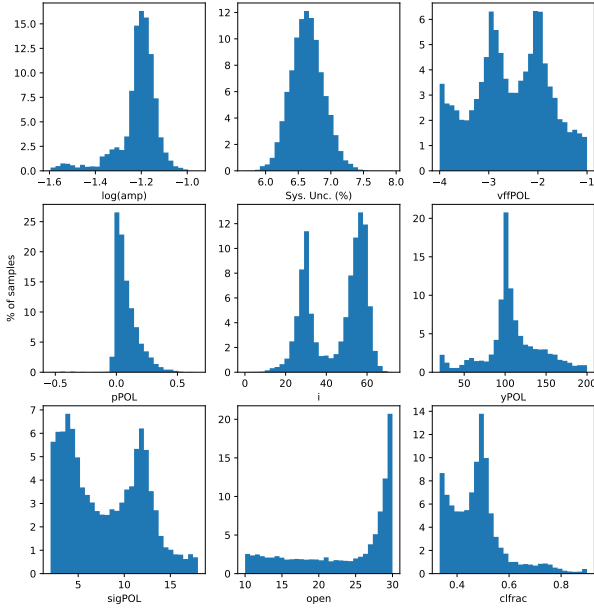


Figure 4. The posterior distribution for the wind of "Torus 1". Produced using the same method as Figure 2 & 3. Note the additional new parameter: f_{cl} , the cloud fraction.

model fits to our data of NGC 3783. Thus, we decided to vary all of the simulation parameters simultaneously. Due to the much larger number of possible models to run we also decided to adopt some priors. [Zach: still already had priors before, just uniform. figure out the right word for what we're adding here] First, we limited the inclination to be $i < 75^\circ$, since for $i > 75^\circ$ NGC 3783 would not have been able to be reverberation mapped (see Section 4). Additionally, we chose to not explore models beyond $Y = 100$ due to the unphysically large clouds that the $Y > 100$ models produce and that these models have never been favored in the previous posteriors. We chose to utilize a fixed cloud fraction of 0.333 (placing 1/3 of the clouds in the torus, with the other 2/3 being evenly distributed in both of the polar bi-cone). Finally, we increased the number of clouds in each simulation from 50,000 to 100,000. All of the parameter values (both varied and fixed) are enumerated in Table ??.

As can be seen in Figure 6, this model set tends to favor a very compact, moderately centrally dense, highly inclined torus with a significantly extended wind. We are able to constrain some of the parameters such as p , p_{pol} , i , Y_{pol} , while other parameters remain unconstrained (Y , $\sigma, \sigma_{\text{pol}}$, $\log(\Phi), \log(\Phi_{\text{pol}})$, and open). Due to the interesting behavior (especially i versus open) at large opening angles and **sigma pol**, the favoring of small $\log(\Phi)$ values, and the large gaps between some of our parameters, we adjusted and re-modeled NGC3783 using altered parameter values, and adding additional "in-between" models to better explore the parameter space around the peak of the posteriors. The parameter values for this new set are enumerated in Table ??, and this set now contains about a million modeled response functions.

This expansion resulted in very few alterations to the best fit parameters, favoring very similar values to the previous set of models.

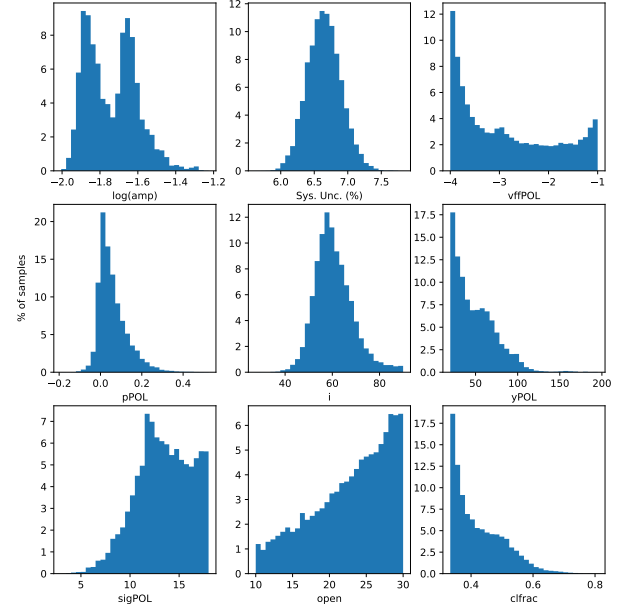


Figure 5. The posterior distribution for the wind of "Torus 2". Compliment to Figure 4, produced using the same method and containing the same parameters.

4 DISCUSSION

In the previous section, we examined the posterior distributions for the structure and geometry of a two component (torus and polar bi-cone) dust distribution model. We found that by increasing the complexity of the model grids used to perform the MCMC search, we were able to better model the IR response of NGC 3783.

4.1 Parameter Estimation of NGC 3783

We find that not all tested parameters have equal impact on the best fit IR response light curve, and are thus more difficult to constrain using this technique. Of the parameters that do most strongly impact the response light curve, we have yet to constrain only some. [Zach: General statement not super useful here. This paragraph almost feels like it should be at the end of this subsection]

We consistently find the strongest constraints for $p(\tilde{\Phi})$ and $p_{\text{pol}}(\tilde{\Phi})$, the radial cloud distribution power law indices. Lower p values tend to result in light curves that respond on too short a time delay resulting in a light curve that is too "sharp". This is likely due to most of the responding clouds being very close to the dust sublimation radius. Conversely, higher p values tend to overly smooth the resulting light curve, with the same justification as for low p values.

The inclination (i) of the distribution is also generally well constrained to moderate inclinations (30° - 60°), with the caveat that completely edge-on models ($i = 90^\circ$) were excluded as priors on the final set of models as they are generally unphysical to reverberation map. Performing reverberation mapping relies on the observer's view of the central source being optically thin to the dust. In edge-on models, the central source would be completely obscured by the torus. These edge-on models, under certain conditions, resulted in degeneracies with models with other less extreme inclinations, motivating their exclusion. We find that inclination has more complex relationships with the other parameters, particularly the opening angle O_{mid} . This

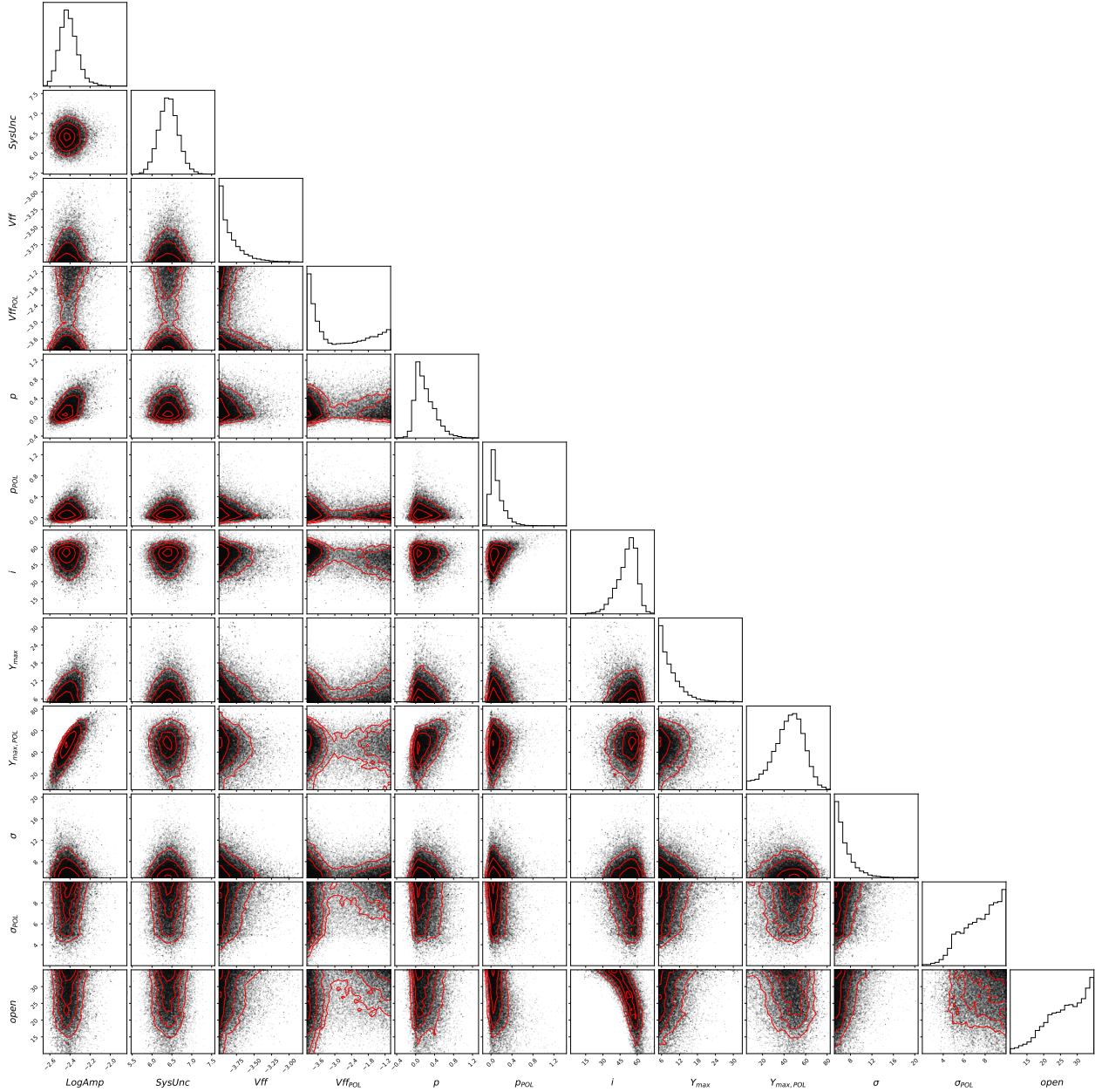


Figure 6. Posteriors of the first set of models which vary both the torus and wind parameters independently. For this set, we choose to visualize both the 1d and 2d posteriors. 2d posteriors are able to show the relationships between parameters, as opposed to just their best fit. Down a column or across a row keeps one of the parameters constant while varying the other parameter. The 1d posteriors are the grid space where both of the parameters are the same. Contour lines for 0.5, 1, 1.5, and 2 sigma are shown.

complexity can likely be attributed to discontinuities between optically thin and optically thick lines of sight to the inner regions of the dust, where the response is strongest.

We find that model grids tend to favor smaller Y values. Hot dust at approximately 1000–2000K responds most strongly in the near-IR H and K bands. Only dust close to the dust sublimation radius ($\lesssim 2R_d$) can reach these temperatures on their illuminated side, suggesting that the best fit Y and Y_{pol} values we find may be more closely related to controlling the overall volume of the dust distribution and thus the cloud sizes. This also suggests that it may be possible to use this technique to further constrain the dust distribution at larger radii using light curves at longer wavelengths. We find that across model grids,

σ and σ_{pol} have a proportionally smaller impact on the response light curve and have not been constrained by our MCMC search. Comparing light curves where σ and σ_{pol} are varied, the shorter timescale features tend to be muted as σ and σ_{pol} increase. However, in further investigations, we would expect the angular width to also relate to the inclination in a similar way to O_{mid} . [Zach: General ideas for this section: Could definitely figure out parameter importances!]

- Previous works generally support the conclusions drawn from "Torus 1" of the variable wind model set.
- It seems that grids must be relatively finely sampled for the influence from a non-delta transfer function to be determined.

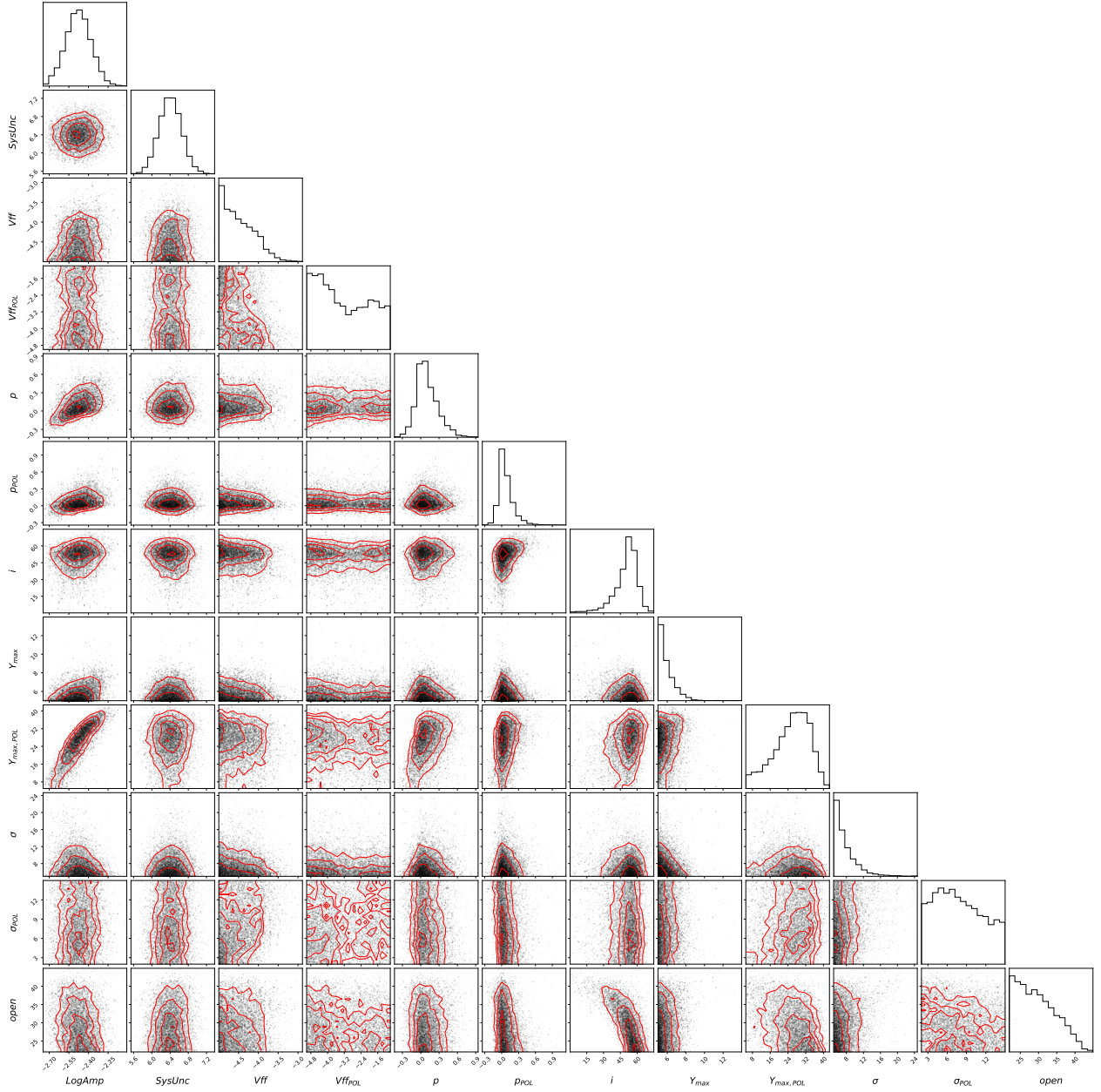


Figure 7. Posteriors of the second set of models varying both the torus and wind independently. Note the change in ranges for some of the parameters.

- The parameter space should only contain feasible models, as non-physical / generally unsupported models can cause degeneracy with feasible models.

4.2 Comparison to Other Models of NGC 3783

Parameter estimates from this technique tend to correlate with predictions made by other methods. IR interferometric observations predict that the torus component of the dust has an inclination that is close to face-on to the observer ($i < 40^\circ$) and a radial extent of $\tilde{0.07}\text{pc}$ for the hot inner edge of the dust (GRAVITY Collaboration 2021). Kinematic simulations of NGC 3783 find a best fit to a polar bi-cone roughly perpendicular to the torus ($i_{\text{pol}} \approx 60\text{-}75^\circ$ with $i_{\text{tor}} \approx 35\text{-}40^\circ$, an offset of $65\text{-}85^\circ$) with $\sigma_{\text{pol}} \approx 7\text{-}10^\circ$, and a half opening angle of

$\tilde{30}\text{-}50^\circ$ (Fischer et al. 2013; Müller-Sánchez et al. 2011). Our models tend to suggest that higher inclination solutions may be allowable, but otherwise our findings are consistent with their results. Dust continuum SED models presented in Hönig and Kishimoto (2017) favor moderate inclinations between 15° and 60° , p values between -1 and 1 , and $p_{\text{pol}} > 1$.

4.3 Limitations & Future Work

4.3.1 Saturation Effects

We now discuss multiple effects which we classify as "saturation effects" as they all have similar effect on the resulting simulated response, namely, at high relative luminosities they each result in

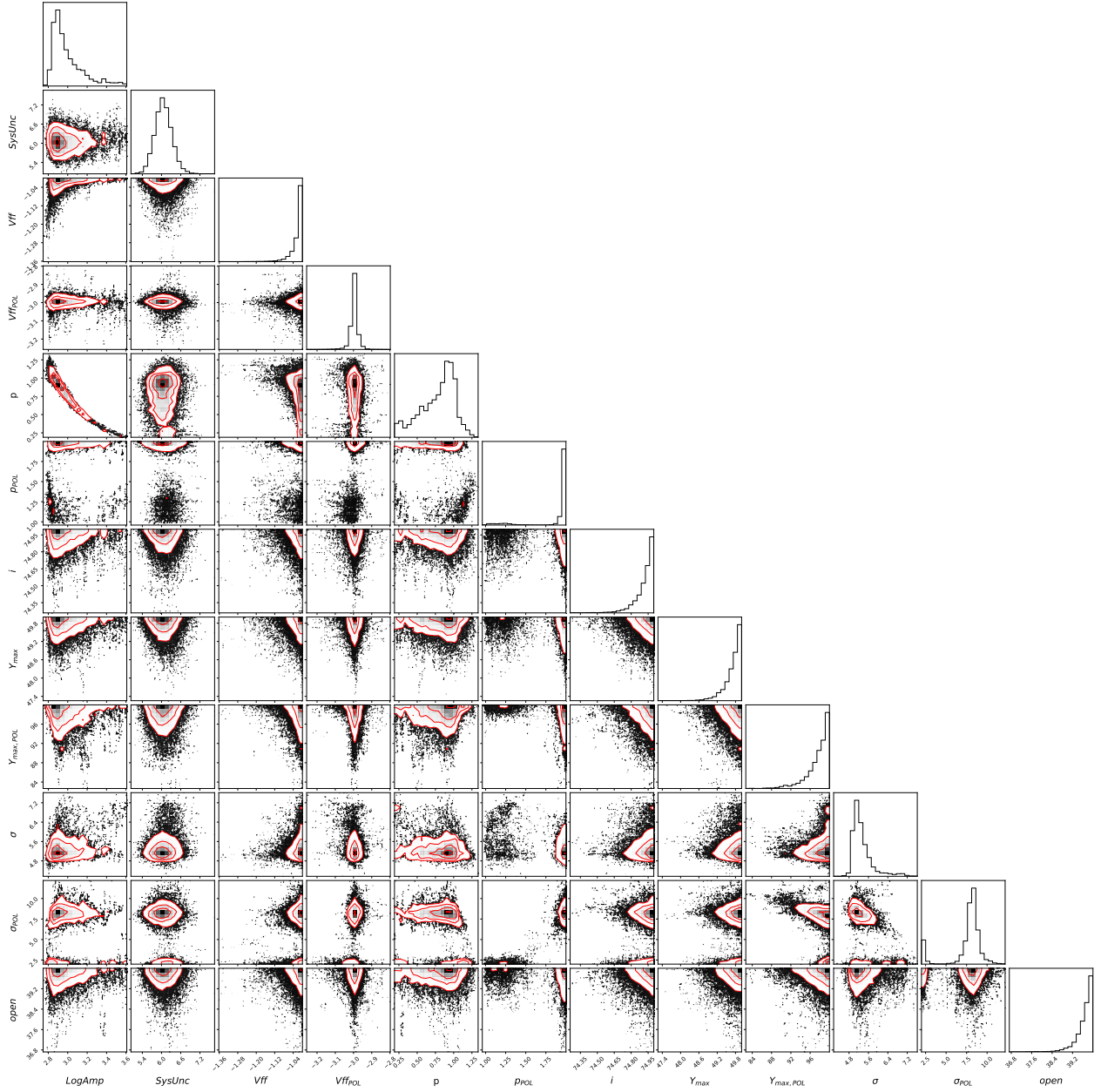


Figure 8. $s0.1, f_{\text{cl}} 0.333$

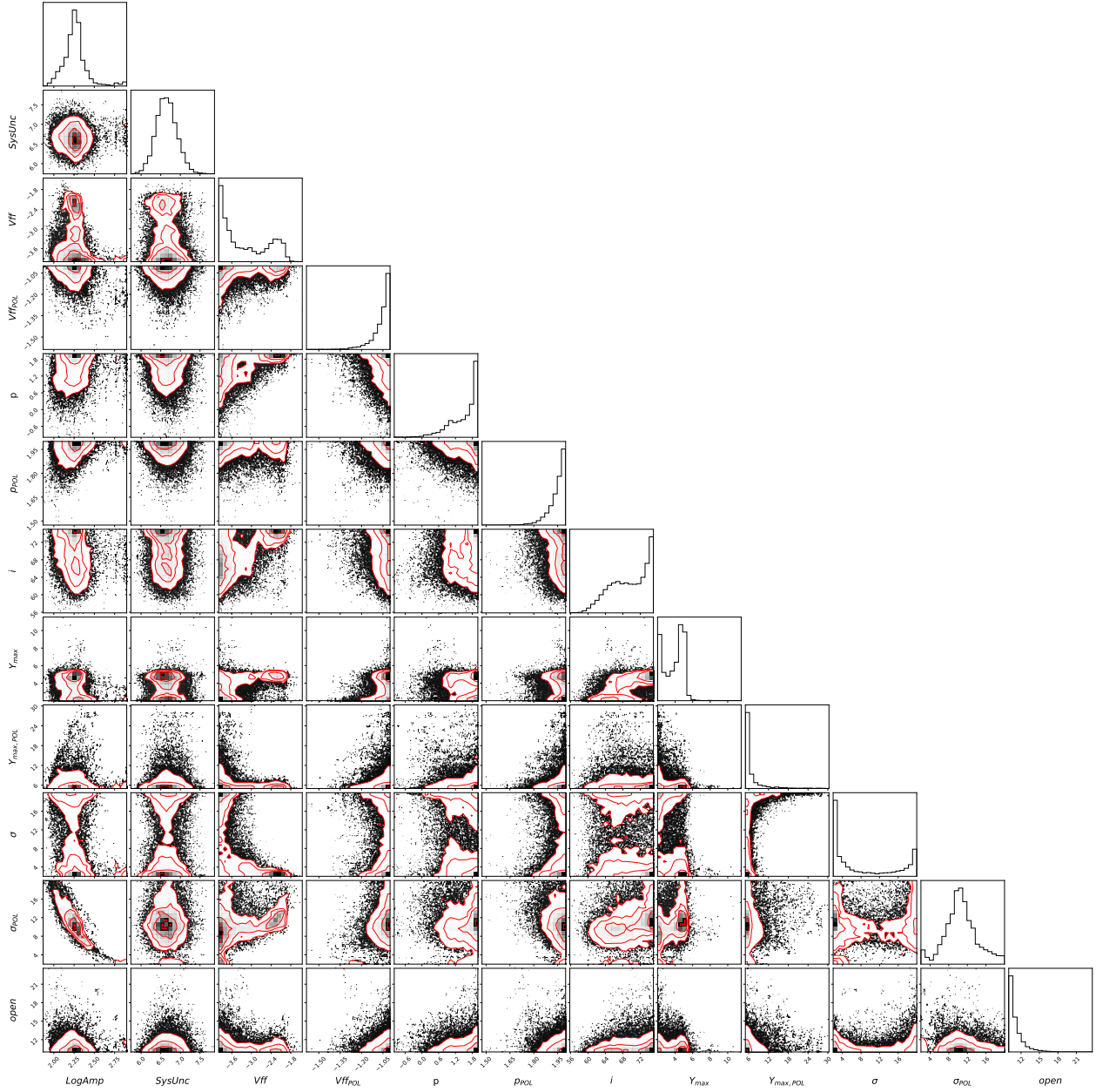
a stunting of the response (saturation) which results in significant deviation from the observed data.

One such effect which is well understood is when clouds become a sufficiently large such that only a small number of clouds ($\lesssim 100$) are able to react directly. This is typically caused by large volume filling factors, large y values, and exacerbated by negative p values. These models are nonphysical due to the clouds' large size particularly at close to the inner edge, but the parameters used may not be nonphysical. This could be addressed by introducing a new parameter to describe the radial dependence of cloud volume, or by significantly increasing the number of clouds in the simulation.

DESCRIBE THE DEVIATION IN FIGURE 5 It is hypothesized that this deviation is caused by the fact that TORMAC currently simulates dust sublimation as a function of temperature only, when in reality it is also a time dependent process. In reality, as clouds at

the inner edge of the dust distribution are pushed inside of the expanding dust sublimation radius, the inner edge of the clouds (which receive the majority of the heating from the central source) begin to sublimate away, while the interior of the cloud raises in temperature. Instead, since TORMAC simply caps the front edge of the cloud at the dust sublimation temperature, the interior of the cloud is capped at a lower temperature than would be expected, resulting in a saturation of the clouds during periods of high emission from the disk.

- Produce more models with similar parameters to those explored in the third set of models, and iteratively refining the results by adding more in-between models.
- Model dust sublimation as a function of luminosity and time, may influence the response at high luminosities
- Model the polar bi-cone as parabolic and or hyperbolic

**Figure 9.** $s1.0, f_{\text{cl}} 0.333$

- Introduce variable cloud size as a function of radius

5 CONCLUSION

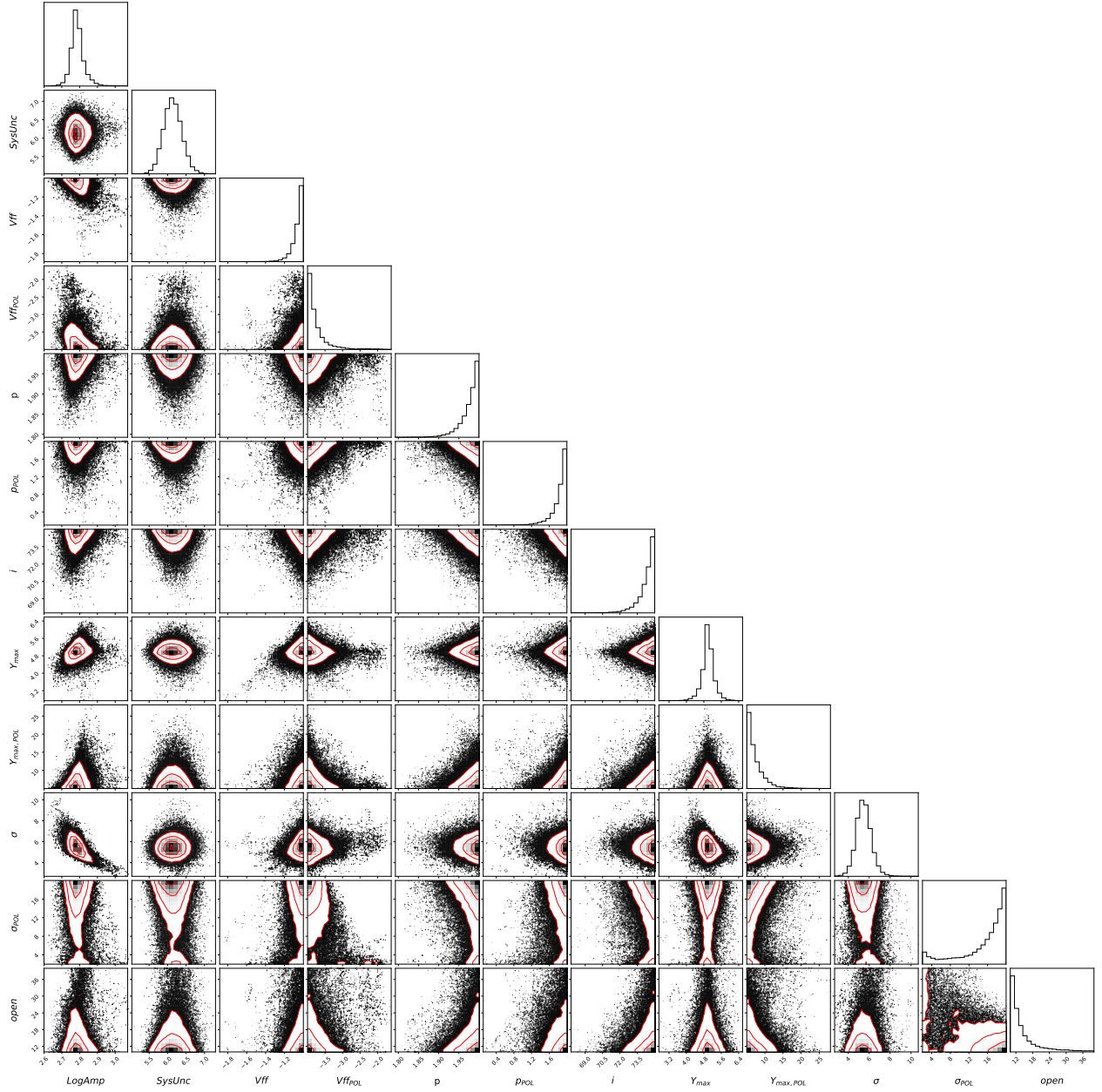
- Torus and polar bi-cone models seem more strongly supported, agrees with observations.
- These models tend to agree with and extend previous attempts to model NGC 3783.
- IR response is very sensitive to some parameters (p, y, vff) but not to others (sig, i).
- Because some parameters have opposite effects on the IR response, it can be difficult to tell some models apart.

ACKNOWLEDGEMENTS

DATA AVAILABILITY

REFERENCES

- Almeyda T., Robinson A., Richmond M., Vazquez B., Nikutta R., 2017, *ApJ*, 843, 3
 Almeyda T., Robinson A., Richmond M., Nikutta R., McDonough B., 2020, *ApJ*, 891, 26
 Lira P., Arévalo P., Uttley P., McHardy I., Breedt E., 2011, *MNRAS*, 415, 1290
 Sales D. A., et al., 2015, *ApJ*, 799, 25


 Figure 10. $s1.0, f_{\text{cl}} 0.667$

APPENDIX A: SOME EXTRA MATERIAL

This paper has been typeset from a TeX/LaTeX file prepared by the author.

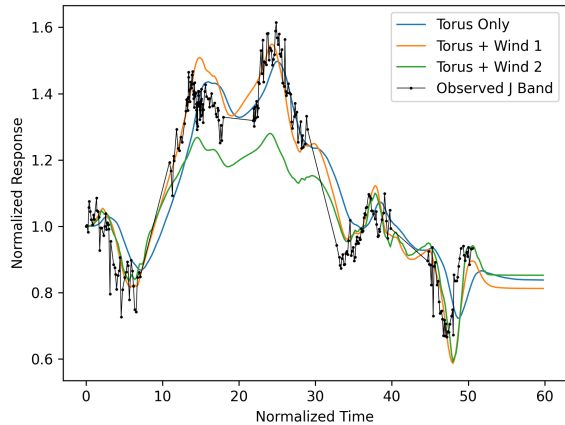


Figure 11. Full TORMAC simulated responses for the best fit torus only model, the best fit torus and bi-cone model (Torus + Wind 1) and the same parameters but with the p parameter modified from 0 to -2 (Torus + Wind 2). Observed $1.25\mu\text{m}$ data from Lira et al. (2011) is also shown.